MULTIBODY DYNAMICS 2005, ECCOMAS Thematic Conference
J.M. Goicolea, J. Cuadrado, J.C. García Orden (eds.)
Madrid, Spain, 21–24 June 2005

AEROELASTIC MODELING AND CONTROL OF WIND TURBINE GENERATORS USING FINITE ELEMENT MULTIBODY PROCEDURES

Carlo L. Bottasso, Alessandro Croce, Barbara Savini, Walter Sirchi, Lorenzo Trainelli

Dipartimento di Ingegneria Aerospaziale
Politecnico di Milano, Via La Masa 34, 20156 Milano, Italy
e-mail: carlo.bottasso@polimi.it,
web page: http://www.aero.polimi.it/~bottasso

Keywords: Multibody Dynamics, Model Predictive Control, Aeroelasticity, Wind Energy, Neural Networks.

Abstract. *In this paper we report on our ongoing research in the area of aeroelastic modeling and control of wind turbine generators. At first we describe a finite element based multibody dynamics code that we use for system modeling and simulation. Next, we formulate an adaptive non-linear model predictive controller. The adaptive element enables the controller to correct the deficiencies of the reduced model used for the prediction, and to self-adjust to changed environmental and operating conditions. In this work we verify the performance of the controller basing the solution of the prediction problem on a direct transcription approach. The tests conducted in this way on gust response and turbulent wind operations provide some benchmark results against which to compare the performance of a real-time neural controller currently under development.*

1 INTRODUCTION

There are strong economic drivers towards the development of large wind turbines that can operate reliably and efficiently with minimum maintenance. Political factors and public acceptance issues push for the installation of such turbines in areas away from human settlements, such as in off-shore farms or in mountainous regions. Environmental factors of such installations make the design and operation of large wind turbines an extremely challenging engineering problem: greater height above ground implies greater risks of coherence turbulence and hence of large dynamic loads transferred to the structure; furthermore, the effects of complex terrains, wind turbulence, and ice accretion, coupled with the large span blades and tall flexible towers of the turbines, render the problem of control of structural vibrations one of the main hurdles in the design and effective installation of such machines.

Therefore, there is a need for developing turbines that can meet the needs of current design configurations, and that can operate in a robust and reliable manner in a wide range of operating conditions for long periods of time with minimum maintenance and monitoring. This paper describes an ongoing research activity in the area of aeroelastic modeling and control of wind turbine generators, to support the above mentioned needs.

The modeling of wind turbine generators is a multi-disciplinary activity that integrates structural dynamics, aerodynamics and control. Our approach is based on a comprehensive finite element based multibody dynamics approach, which serves as integrator of the various disciplines. Structural elements, joints, actuators and electro-mechanical elements defined in the code library can be assembled to describe arbitrary turbine configurations, which also include mathematical models of the on-board sensors. The aerodynamic models include IEC deterministic and stochastic winds, and the modeling of effects such as rotor-nacelle-tower interactions, upwind turbine shadowing and ice accretion. The control modules include supervisor models and feedback controllers. Different control strategies are available within the code control library, ranging from simple proportional-integral-derivative controllers to highly sophisticated neural-adaptive model-predictive ones. The software includes procedures for optimizing controller performance in terms of fatigue damage to the structure and power efficiency.

The paper discusses the capabilities and functionalities of the code, which are demonstrated by means of relevant problems.

2 OVERVIEW OF THE FINITE ELEMENT MULTIBODY CODE

In this work we use a finite element based multibody formulation that is more thoroughly described in Reference [4]. The code, inspired and partially based on a software tool that was originally developed for rotorcraft applications, includes specific features useful for the modeling of wind turbines. One of the main highlights of the code is its generality: in fact, no assumption is made a priori about the topology of the model. Rather, one can assemble the model by connecting elements from a library that includes body models (beams and rigid bodies), mechanical joints (including the lower pairs, unilateral contact conditions, and flexible joints), actuators (including prescribed displacements and rotations within joints, first order and second order actuator dynamics models, generator models, etc.). Since each element from the library can be connected to any other element, even by forming closed loops, wind turbine generators of arbitrary topology can be modeled.

The multibody formulation is based on the full finite element method, which means that no modal based reduction is performed on the deformable components of the structure. Cartesian coordinates are used for the description of all entities in the model, and all degrees of freedom

are referred to a single inertial frame; this avoids the introduction of multiple floating frames, and leads to a geometrically exact formulation, i.e. a formulation that handles arbitrarily large three dimensional rotations.

The turbine blades and tower are modeled by beam elements. The element models beams of arbitrary geometry, including curved and twisted reference lines, and accounts for axial, shear, bending and torsional stiffness.

Joints are modeled through holonomic or non-holonomic constraints, as appropriate, which are enforced by means of Lagrange multipliers using the augmented Lagrangian method. All joints can be equipped with internal springs, dampers, backlash, and friction models.

Lifting lines can be associated with beam elements and are described by three dimensional twisted curves, which do not necessarily coincide with the associated beam reference lines. The lifting lines are based on classical two-dimensional strip theory and use local profile aerodynamic characteristics, accounting for the aerodynamic center offset, twist, sweep, and unsteady corrections. Lifting lines are here used to model the aerodynamic characteristics of the blades, but also of the tower and of the nacelle. An inflow element can be associated with the blade lifting lines to model the rotor inflow effects; presently, the Peters-He [11] and the dynamic Pitt-Peters wake models [12] are implemented in the code.

Wind is modeled as the sum of a steady state mean wind and a perturbation wind, accounting for turbulence and/or gusts. The deterministic component of the wind field implements the transients specified by IEC 61400-1 [1], the exponential and logarithmic wind shear models, and the tower shadow effects, which include the potential flow model for a conical tower, the downwind empirical model based on Reference [13], or an interpolation of these two models. The stochastic component of the wind field is computed according to the Von Karman and Kaimal turbulence models. The turbulent wind is pre-computed before the beginning of the simulation for an assigned duration of time and for a user-specified two-dimensional grid of points. During the simulation, the current position of each airstation is mapped to this grid, and the current value of the wind is interpolated in space and time from the saved data.

The multibody formulation used in this effort leads to a set of non-linear partial differential algebraic equations. Spatial discretization of the flexible components using the finite element method yields a system of differential algebraic equations in time, which are solved using an implicit integration procedure which is non-linearly unconditionally stable. The implicit nature of the scheme allows for the use of large time steps and is more appropriate than explicit schemes for the typical dynamics of rotor systems. At each time step, the resulting non-linear system of equations is solved using a quasi-Newton scheme. The time step length is adjusted based on an error indicator. Ad hoc procedures are used for refining the step during intermittent contact events, for example when a backlash contact model is present in a joint.

The proof of non-linear unconditional stability of the scheme stems from two physical characteristics of multibody systems that are reflected in the numerical scheme at the discrete level: the preservation of the total mechanical energy and the vanishing of the work performed by constraint forces. Numerical dissipation, which is important when dealing with stiff differential algebraic systems and with high frequency unresolved modes, is obtained by letting the solution drift from the constant energy manifold in a controlled manner in such a way that at each time step, energy can be dissipated but not created. More details on these non-linearly stable schemes can be found in the bibliography of Reference [4] and in [3].

The code can perform several different analysis types. A static analysis solves the static equations of the problem, obtained by setting all time derivatives to zero, yielding the deformed structural configuration under steady loads. The steady loads include prescribed external forces,

steady aerodynamic loads or inertial loads due to rotation of elements of the system at constant prescribed angular velocity. An eigenanalysis can be performed about the deformed equilibrium configuration, to yield the natural frequencies and eigenmodes of the linearized system response about this configuration.

Typically, a static analysis is used for computing consistent initial conditions for a subsequent dynamic analysis. The user can specify a number of sensors on the virtual prototype of the turbine, which provide output information for the analysis. The same sensor outputs can also be fed as inputs to the on-board controllers, which in turn operate the system actuators. Controllers, which can include supervision logics and feedback controllers, are implemented as user-defined routines that are linked with the rest of the code.

Finally, the model preparation and data interpretation phases are supported by various graphic procedures, including animations and time history plots, and other post-processing operations such as the determination of fatigue loads by a rainflow analysis.

3 NON-LINEAR MODEL PREDICTIVE CONTROL OF WIND TURBINES

In this project, we are exploring the applicability to wind turbines of non-linear model predictive control (NMPC) theory [9]. References [14] and [15] report of well over two thousand successful industrial implementations of linear and non-linear model predictive control. The technology can be considered by now mature, and is best suited for difficult control problems, where maximum performance is required and were classical control design approaches fail.

A model predictive controller predicts the future behavior of the plant using a reduced model, and finds the control actions necessary for regulating the plant solving an optimal control problem on a receding horizon. The reduced model used for prediction can be augmented with an adaptive neural element, whose role is to correct the deficiencies of the reduced model with respect to the actual plant.

The basic principle of non-linear model-predictive control is illustrated in Figure 1. A non-linear reduced model of the wind turbine is used for predicting the future behavior of the plant under the action of the control inputs $\boldsymbol{u}$, which are typically represented by the pitch settings of the rotor blades and by the generator torque. An open-loop optimal control problem is solved for the reduced model on a finite horizon (the prediction window $[t, t + T_p]$). The cost of this optimization problem is a function of the error in the desired target value, for example a desired value of the rotor speed.

The controls computed by the optimizer are now used for steering the plant, but only on a short time horizon up to time $t + T_s$, as soon as a new measurement becomes available. In fact, due to the presence of disturbances, such as wind turbulence, and the inevitable mismatch between reduced model and plant, the actual outputs will drift away from the predicted ones. Once the plant has reached the end of the steering window $[t, t + T_s]$ under the action of the computed control inputs, the model-predictive optimization problem is solved again, looking ahead in the future over the prediction horizon shifted forward in time. This procedure results in a feedback, receding horizon approach.

The future control actions are computed by solving the following open-loop optimal control

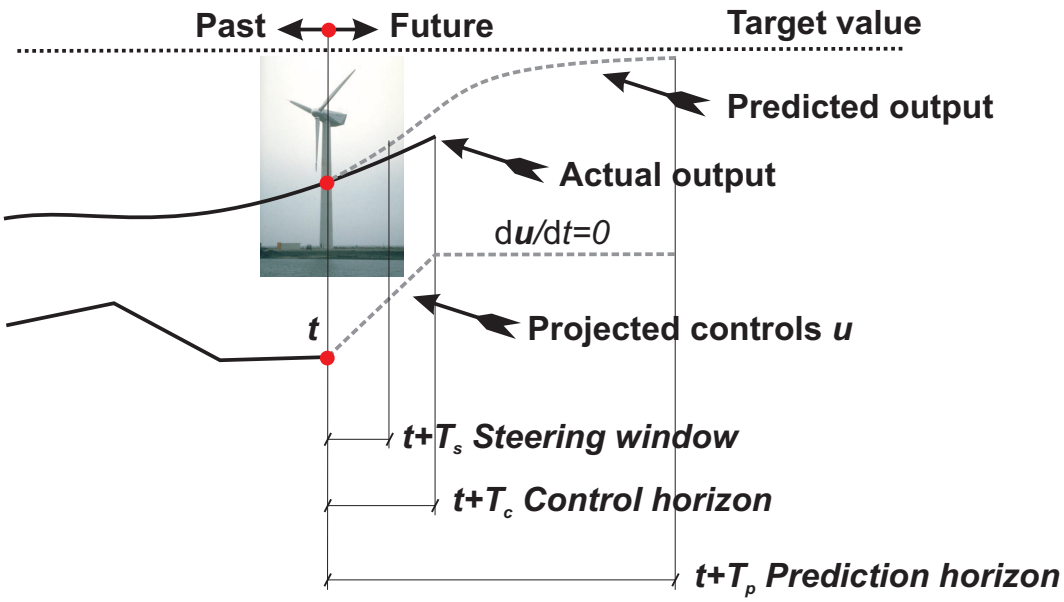

Figure 1: Model-predictive control of wind turbines.

problem:

$$\min_{\boldsymbol{y},\boldsymbol{u}} J, \tag{1a}$$

$$\text{with: } J = \int_t^{t+T_p} F(\boldsymbol{y}(\tau), \boldsymbol{u}(\tau), \boldsymbol{y}^*, \boldsymbol{u}^*)\mathrm{d}\tau, \tag{1b}$$

$$\text{s.t.: } \boldsymbol{f}(\dot{\boldsymbol{y}}, \boldsymbol{y}, \boldsymbol{u}) = 0, \tag{1c}$$

$$\boldsymbol{g}(\boldsymbol{y}(\tau), \boldsymbol{u}(\tau)) \in [\boldsymbol{g}_{\min}, \boldsymbol{g}_{\max}] \quad \forall \tau \in [t, t+T_c], \tag{1d}$$

$$\dot{\boldsymbol{u}}(\tau) = 0 \quad \forall \tau \in [t+T_c, t+T_p]. \tag{1e}$$

Goal of the optimization problem is to bring the system to the target regulation set point $\boldsymbol{y}^*$ in an optimal way, while satisfying all constraints. The solution of the optimization problem is obtained through the prediction of the response of the plant, as described by a non-linear reduced model given by Eq. (1c).

The optimization satisfies possible constraints and bounds on the states and controls, expressed collectively by Eq. (1d). These constraints can include, for example, limited control authority and bounds on the pitch command and its rates, or maximum values of important parameters of the system that need not to be exceed, as for example maximum loads in critical parts of the structure.

The regulation cost J can be selected to provide specific performance characteristics to the controller. In this work the cost is defined as the integral over the prediction window of the function

$$F(\boldsymbol{y}, \boldsymbol{u}, \boldsymbol{y}^*, \boldsymbol{u}^*) = (\boldsymbol{y}-\boldsymbol{y}^*)^T \boldsymbol{Q}(\boldsymbol{y}-\boldsymbol{y}^*) + (\boldsymbol{u}-\boldsymbol{u}^*)^T \boldsymbol{R}(\boldsymbol{u}-\boldsymbol{u}^*), \tag{2}$$

where the first term accounts for the regulation error $\boldsymbol{y}-\boldsymbol{y}^*$, while the second term is typically used for limiting the activity of the controller, being $\boldsymbol{u}^*$ a reference value for the control.

In this work, the reduced model used for predicting the future behavior of the plant includes an adaptive element, following [6, 7]. Hence the reduced model is composed of a reference model augmented by a neural network that provides for the adaption capabilities, and is written

$$\boldsymbol{f}_{\text{ref}}(\dot{\boldsymbol{y}}, \boldsymbol{y}, \boldsymbol{u}) = \boldsymbol{d}(\dot{\boldsymbol{y}}, \boldsymbol{y}, \boldsymbol{u}). \tag{3}$$

In the previous equation, $\boldsymbol{f}_{\text{ref}}(\dot{\boldsymbol{y}}, \boldsymbol{y}, \boldsymbol{u})$ is a reference model of the wind turbine, which is described in Section 3.1, while $\boldsymbol{d}(\dot{\boldsymbol{y}}, \boldsymbol{y}, \boldsymbol{u})$ is the reference model defect.

If one knew the function $\boldsymbol{d}$, the prediction of the system states $\boldsymbol{y}$ would exactly match the corresponding values of the plant. In other words, the defect is that unknown function that ensures a perfect matching between the states $\boldsymbol{y}$ of the reduced model and the corresponding states of the plant. The idea is now to approximate the defect $\boldsymbol{d}$ using a single-hidden-layer neural network:

$$\boldsymbol{d}(\dot{\boldsymbol{y}}, \boldsymbol{y}, \boldsymbol{u}) = \boldsymbol{d}_{NN}(\dot{\boldsymbol{y}}, \boldsymbol{y}, \boldsymbol{u}) + \boldsymbol{\varepsilon}, \tag{4}$$

with

$$\boldsymbol{d}_{NN}(\dot{\boldsymbol{y}}, \boldsymbol{y}, \boldsymbol{u}) = \boldsymbol{W}^T \boldsymbol{\sigma}(\boldsymbol{V}^T \boldsymbol{x} + \boldsymbol{a}) + \boldsymbol{b}, \tag{5}$$

where $\boldsymbol{x} = (\dot{\boldsymbol{y}}^T, \boldsymbol{y}^T, \boldsymbol{u}^T)^T$ are the network inputs, $\boldsymbol{W}$ and $\boldsymbol{V}$ are matrices of synaptic weights, $\boldsymbol{a}$ and $\boldsymbol{b}$ are the network biases, and

$$\boldsymbol{\sigma}(\boldsymbol{\phi}) = (\sigma(\phi_1), \ldots, \sigma(\phi_{N_h}))^T$$

is the vector-valued function of sigmoid activation functions $\sigma(\bullet)$ for the N_h processing elements in the hidden layer. The universal approximation property of neural networks [10] ensures that the functional reconstruction error $\boldsymbol{\varepsilon}$ in Eq. (4) can be bounded as $||\boldsymbol{\varepsilon}||_2 \leq C_\varepsilon$ for any $C_\varepsilon > 0$, for some appropriately large number of hidden neurons N_h, assuming that $\boldsymbol{d}$ is sufficiently smooth.

The neural network is trained with an error-correction learning algorithm, whereby the network parameters are adjusted to minimize the error between the network output and the desired output [8]. This way, the reduced model, and hence the controller, can self-adjust to specific situations. For example, different installations of the same model of a wind turbine generator will be subjected to different local environmental conditions, such as shadow effects due to the presence of neighboring turbines or due to specific morphological characteristics of the terrain. A model predictive controller augmented with an adaptive neural network can learn how to compensate for these different effects, thereby optimizing the performance of the closed-loop system to each specific installation or environmental condition.

Training, i.e. ensuring a proper matching between predicted and actual outputs, can be obtained by subjecting reduced model and plant to the same control actions, and by tuning the reduced model parameters so that some measure of mismatch between the two is minimized. Indicating with $\boldsymbol{u}^o$ the optimal control inputs computed at time t on the basis of problem 1 and with $\widetilde{\boldsymbol{y}}$ the resulting response of the plant in the steering window $[t, t + T_s]$, then the neural network approximation error of the unknown defect function is computed based on Eq. (3) and (4) as

$$E = ||\boldsymbol{f}_{\text{ref}}(\dot{\widetilde{\boldsymbol{y}}}, \widetilde{\boldsymbol{y}}, \boldsymbol{u}^o) - \boldsymbol{d}_{NN}(\dot{\widetilde{\boldsymbol{y}}}, \widetilde{\boldsymbol{y}}, \boldsymbol{u}^o)||_2. \tag{6}$$

This error is approximatively minimized using the back-propagation algorithm [16]: the local information provided by the last steering of the plant is used for correcting the current estimate $\boldsymbol{p} = (\ldots, W_{ij}, \ldots, V_{ij}, \ldots, a_i, \ldots, b_i, \ldots)^T$ of the network parameters as

$$\boldsymbol{p} = \boldsymbol{p} + \Delta\boldsymbol{p}, \tag{7}$$

where $\Delta\boldsymbol{p}$ is the steepest-descent search direction

$$\Delta\boldsymbol{p} = -\eta \frac{\partial \int_t^{t+T_s} E \, \mathrm{d}t}{\partial \boldsymbol{p}}, \tag{8}$$

and η is the learning rate.

The solution of the model predictive regulation problem (1) can be approximated in two alternative ways: through a numerical method, or by training of a second neural network (neural control). The two approaches have different characteristics. The latter is less computationally intensive and has the potential for achieving real-time performance even in the presence of limited on-board computational resources. On the other hand, the training of the control network can be problematic because of the very large dimension of the solution space. Furthermore, one can not deal directly with possible input and output constraints (Eq. (1d)), which are on the contrary trivially accounted for with the numerical solution approach.

Our long term objective for this research project is the development of robust and reliable neural control schemes that achieve real-time performance. While work in this direction is well underway, in this paper we restrict our attention to the sole numerical solution approach. Based on the above comparison between the two approaches, it can be argued that a predictive neural controller can only approximate the performance of a predictive controller based on a numerical method. Hence, the result of the investigation of this paper provides the upper bounds in terms of performance which are achievable by a model predictive controller. This, in turn, will represent the benchmark against which to compare the neural controller in a forthcoming work.

The solution to the model predictive regulation problem is here obtained by the direct transcription method [5]. The governing equations of the reduced model are discretized on a computational grid of the prediction window using an appropriate numerical method. This defines a set of discrete unknown state and control parameters on the computational grid. Next, the constraint conditions and the problem cost function are expressed in terms of the discrete parameters. This in turn defines a non-linear discrete parameter optimization problem, i.e. a Non-Linear Programming (NLP) problem, that is solved using a sequential quadratic programming (SQP) approach [2]. The numerical solution of the discrete problem approximates the solution of its infinite-dimensional counterpart, problem (1). In this work, the transcription process is based on the implicit mid-point rule.

3.1 Reduced wind turbine model

The non-linear reduced reference model of the turbine includes drive-train shaft dynamics, elastic tower fore-aft motion and blade pitch actuator dynamics, and it is written

$$(J_R + J_G)\dot{\Omega} + Q_l(\Omega) + Q_{el}(\Omega) - Q_a(\dot{x}, \Omega, \beta_e, V_w, t) = 0, \tag{9a}$$

$$M_T\ddot{x} + C_T\dot{x} + K_T x - F_a(\dot{x}, \Omega, \beta_e, V_w, t) = 0, \tag{9b}$$

$$\ddot{\beta}_e + 2\xi\omega\dot{\beta}_e + \omega^2(\beta_e - \beta_c) = 0. \tag{9c}$$

The first equation, Eq. (9a), describes the drive-train dynamics. Ω is the rotor angular velocity, x is the tower tip fore-aft displacement and β_e is the effective blade pitch angle. Moreover, J_R is the sum of the moments of inertia about the rotation axis of the rotor hub and of the rotor blades, while J_G is the moment of inertia of the rotating part of the electric generator. The torques acting upon the drive-train include the mechanical losses on the shaft bearings Q_l, the electrical reaction torque Q_{el} and the aerodynamic torque Q_a. The mechanical loss Q_l is modeled by means of a speed-torque look-up table, while the electrical torque Q_{el}, modeled by means of a speed-power look-up table augmented by a term proportional to the rotor acceleration, includes a time delay to account for the dynamics of the electric generator.

The second equation, Eq. (9b), models the fore-aft tower dynamics. Here, M_T, C_T and K_T are, respectively, the tower equivalent modal mass, structural damping and bending stiffness. These quantities are in this work obtained by modal reduction of a detailed finite element model of the tower. Finally, F_a indicates the aerodynamic force produced by the rotor.

The third and last equation, Eq. (9b), is a second order model of the blade pitch actuator, where ω is the undamped natural frequency, ξ the damping factor, and β_c the blade pitch control. The model also includes upper and lower limits on the pitch and the pitch rate: $\beta_c \in [-1.5, 85]$ deg, $\dot{\beta}_c \in [-11, 11]$ deg/sec. Although a rotor will have a pitch actuator for each blade, for simplicity we suppose here that they will be operated with the same pitch input. However, it is clear that the present approach is suited to cyclic pitch control without any modification, a part from the writing of Eq. (9c) for each blade.

The aerodynamic force and torque acting on the rotor are computed as

$$Q_a = \frac{1}{2}\,\rho\pi R^3 \frac{C_P(\lambda,\beta_e)}{\lambda}(V_w - \dot{x})^2, \tag{10a}$$

$$F_a = \frac{1}{2}\,\rho\pi R^2 C_F(\lambda,\beta_e)(V_w - \dot{x})^2, \tag{10b}$$

where ρ is the air density, C_P and C_F the effective power and force coefficients, respectively, and λ is the tip-speed ratio, defined as

$$\lambda = \frac{\Omega R}{V_w - \dot{x}}. \tag{11}$$

Finally, V_w is the turbulent upstream wind speed. In the current implementation of the reduced model, an estimate of the wind velocity is obtained from a wind sensor placed at the hub. The mean wind is held constant throughout the prediction window and equal to the last available measurement. Therefore, the time-dependence of the wind is recovered through the controller sampling. It would be relatively straightforward, but it was not attempted in this work, to include more sophisticated extrapolation schemes for the wind speed.

The aerodynamic coefficients were obtained off-line from simulations performed using the multibody model, considering steady wind conditions. The coefficients are computed on-line in terms of effective blade pitch angle and tip-speed ratio by means of look-up tables.

Given the above definition of the reduced reference model, the state vector $\boldsymbol{y}$ of problem (1) is defined as $\boldsymbol{y} = (\Omega, x, \dot{x}, \beta_e, \dot{\beta}_e)^T$, while the control is $u = \beta_c$. Accordingly, the reference model equations $\boldsymbol{f}_{\text{ref}}$ of (3) are obtained by putting Eq. (9) in first order form. The defect correction $\boldsymbol{d}$ of Eq. (3) acts only on the drive train dynamics and on the fore-aft tower dynamics, which are the dynamic equilibrium equations most affected by modeling errors with respect to the plant.

4 RESULTS

In this work we consider a wind turbine in the 1.2 kW class, with a three-bladed rotor with blade pitch and generator torque control. The rotor has a radius R=38.3 m, an up-tilt of 5 deg, and no pre-cone. A detailed multibody model of the turbine was developed using the formulation of Section 2, which includes flexible blades and tower, flexible tower foundations, hub, drive shaft, flexible drive train accounting also for mechanical losses on the shaft bearings, nacelle, generator, and pitch actuators. Aerodynamic effects are modeled as previously discussed by means of appropriate lifting lines on the various bodies of the structure, including an inflow element for the rotor disk, and turbulent wind models.

The model is equipped with various sensors. Rotor angular velocity, tower tip displacement and velocity, and pitch actuator rotation and rotational speed sensors provide the plant quantities that match the reduced model states $\boldsymbol{y}$. The effect of the rotor speed transducer is accounted for by means of a time lag of 0.01 sec. Furthermore, the transducer measurement is fed into a fourth-order Butterworth filter with a cut-off frequency of 1.27 Hz, which is the frequency with which the rotor blades sample the tower at a rated rotor speed of 18.5 rpm. Filters of this sort are commonly used to eliminate deterministic fluctuations of the rotor speed induced by tower shadowing and wind shear phenomena, and this effect is here included for increased modeling fidelity. Finally, force sensors at the blade roots and along the tower provide information on the state of stress of the structure at these locations.

First, to illustrate some of the modeling capabilities of the aeroelastic code, we consider the dynamic response on the wind turbine subjected to the design load case 1.5 as specified by IEC 61400-1 [1]. In this design situation, the wind turbine, running and connected to the electric load, is subjected to the 1-year extreme operating gust (EOG_1) with an initial magnitude of 10.6 m/sec. In order to consider a worst-case scenario, a loss of electrical connection is further assumed to take place 1 sec before the beginning of the gust. In this situation, the supervisor control system applies an emergency shut down, feathering the blades at the maximum allowable pitch rate in order to reduce the rotor speed and the load peaks. The time history of the rotation of one of the blades is shown in Figure 2 at left, while the same figure on the right shows the resulting local components of the internal reaction forces at the root of the same blade. Figure 3 presents a snapshot of the rotor multibody model during the simulation. Arrows on the blades depict the instantaneous distribution of aerodynamic forces along the lifting lines.

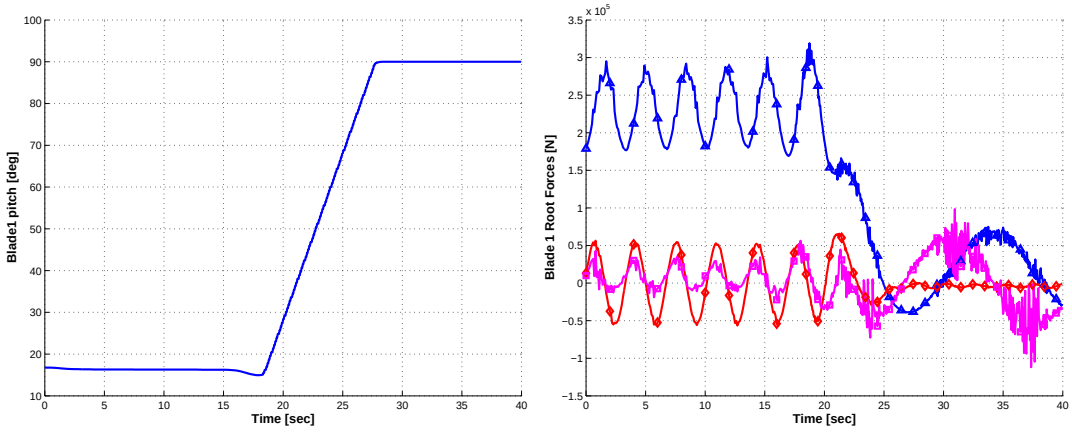

Figure 2: Design load case 1.5 of IEC 61400-1 [1]. At left, time history of blade pitch. At right local components of the internal reaction forces at the blade root.

Next, we illustrate the basic capabilities of the NMP controller based on the formulation of Eqs. (1) in a few representative operational conditions. In the cost function definition, Eq. (2), we set $\boldsymbol{y}^* = (\Omega^*, 0, \beta_e^*, 0)^T$, where $\Omega^* = 1.94$ rad/sec is the standard operating angular velocity in region 2, and β_e^* is the corresponding peak power pitch angle which is a function of the mean wind speed.

To provide for a direct comparison of the model predictive controller with conventional approaches, we have also implemented a proportional-integral-derivative (PID) controller. The

Figure 3: Rotor multibody model.

PID control strategy is to calculate the blade control input β_c as

$$\beta_c = K_p(\Omega - \Omega^*) + K_i \int_0^t (\Omega - \Omega^*)\,\mathrm{d}\tau + K_d\dot{\Omega}, \tag{12}$$

where K_p, K_i and K_d are the proportional, integral and derivative gains, respectively. Optimal gains for the PID controller were obtained by first parameterizing the operating conditions in terms of mean wind speed. We considered 5 equally spaced conditions in the range $V_m \in [13, 25]$ m/sec. Next, for each operating point simulation runs were performed for a duration of 220 sec in Category A turbulence for a grid of control gain values and for a fixed value of the derivative gain. For each combination of proportional and integrals gains, we computed the cost function of Eq. (2), then an average cost was obtained by weighting the costs computed for each operating condition with the Rayleigh wind probability distribution

$$f(V_m) = \frac{\pi V_m}{2V_R^2}\, e^{-\pi\left(\frac{V_m}{V_R^2}\right)^2}, \tag{13}$$

around a medium wind value $V_R = 12$ m/sec. Finally, this average cost was plotted on a two dimensional chart as a function of the gains. The optimal gain values K_i^* and K_p^* for a specific derivative gain were determined by inspection of the charts, for example Figure 4 shows the optimal solution for $K_d = 4$. Finally the optimal combination is determined by finding the minimum with respect to the derivative gain, as shown in Figure 5.

4.1 Gust response

At first, we consider the dynamic response of the plant subjected to EOG_1 [1]. The deterministic wind V_m, initially equal to $V_m^* = 13$ m/sec, reaches its peak in about 5 sec, and

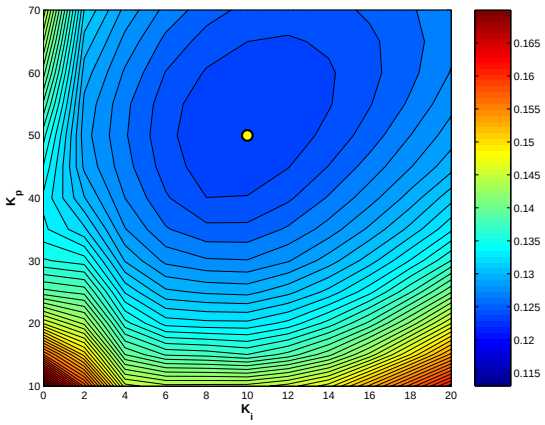

Figure 4: Chart of the cost function J of Eq. (2), averaged throughout the mean wind range $V_m \in [13, 25]$ m/sec, as a function of the PI control gains, for a fixed $K_d = 4$.

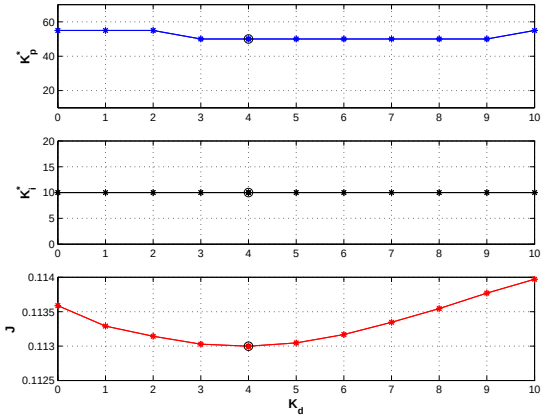

Figure 5: Cost function and optimal proportional and integral gains with respect to the derivative gain. The marker shows the best combination.

then decreases back to its initial value. Figure 6 shows the NMPC solution (solid line) and the PI solution (dashed line) in terms of the non-dimensional rotor speed Ω/Ω^*. The same figure shows also the non-dimensional gust speed V_m/V_m^* as a function of time, plotted using a thin solid line. It appears that the two controllers have quite similar performance, both in terms of response time and of over and under-shoots.

The situation is different for the extreme coherent gust (ECG) [1], with wind speed changing from a value of 10.6 m/sec (cut-out value) to 25 m/sec in 10 sec. Figure 7 shows the NMPC solution (solid line) and the PI solution (dashed line) in terms of the non-dimensional rotor speed Ω/Ω^*. The gust time history, which is superimposed to the response even in this case, highlights the fact that the model predictive controller is able to regulate the system back to its nominal operating condition very soon after the termination of the gust. Notice also from the same plot that this controller shows a substantially reduced over-shoot with respect to the PI solution, notwithstanding the use of optimal gains.

4.2 Operations in turbulent constant-mean wind

Next, we evaluate the performance in turbulent constant-mean wind. Dynamic simulations were conducted for a duration of 300 sec under constant values of the mean hub-height wind speed (ranging between 13 m/sec and 22 m/sec) and Category A turbulence.

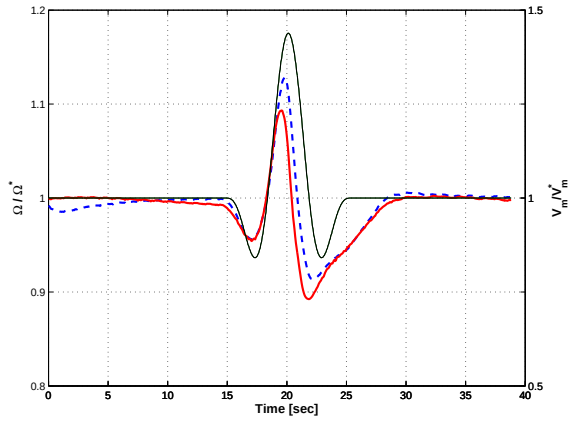

Figure 6: Time history of non-dimensional rotor angular speed Ω/Ω^* for the EOG_1 gust. NMPC solution: solid line; PI solution: dashed line; thin solid line: deterministic non-dimensional gust speed V_m/V_m^*.

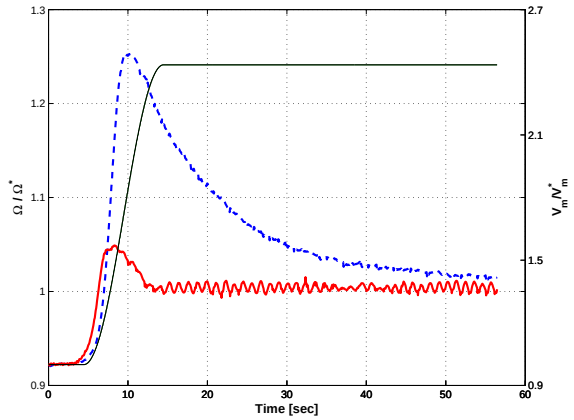

Figure 7: Time history of non-dimensional rotor angular speed Ω/Ω^* for the ECG gust. NMPC solution: solid line; PI solution: dashed line; thin solid line: deterministic non-dimensional gust speed V_m/V_m^*.

Figure 8 reports the standard deviation of the non-dimensional rotor speed error $\Omega/\Omega^* - 1$ as a function of the mean hub-height wind speed for Category A turbulence. It appears that the predictive controller is capable of more than halving the angular velocity fluctuations with respect to the PID controller. At 13 m/sec this improvement is less marked, probably because the turbulent fluctuations can cause wind speeds so low that the target rotor speed can not be achieved no matter what controller one is using.

A more constant value of the rotor speed has a positive influence on the generation of power. This point is made clear by Figure 9 which, for the same operating conditions of the previous figure, shows the standard deviation of non-dimensional generated power. Here again a substantial performance improvement denoted by smaller fluctuations is apparent for the predictive approach with respect to the PI controller.

5 CONCLUSIONS

We have described an ongoing research effort in the area of modeling and control of modern wind turbines. The aeroelastic modeling of the system is based on a multibody finite element based approach that allows for the detailed representation of complex systems of arbitrary topology.

This code has been integrated with advanced neural-adaptive model predictive feedback con-

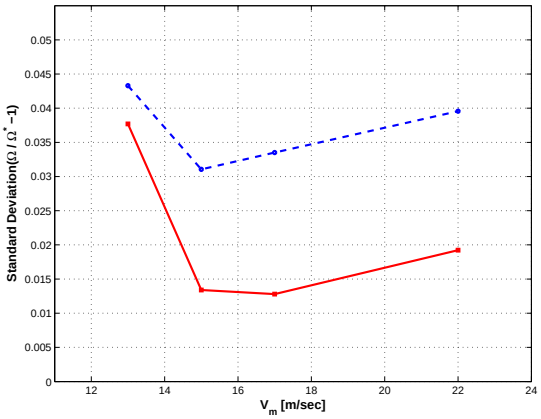

Figure 8: Standard deviation of non-dimensional rotor speed error vs. mean hub-height wind speed for Category A turbulence. NMPC solution: solid line; PI solution: dashed line.

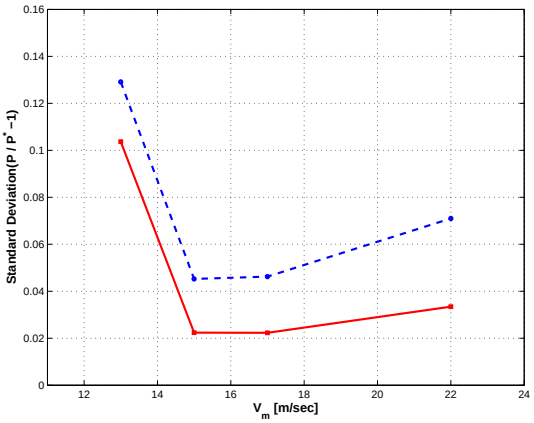

Figure 9: Standard deviation of non-dimensional generated power vs. mean hub-height wind speed for Category A turbulence. NMPC solution: solid line; PI solution: dashed line.

trollers. The prediction of the future behavior of the turbine is based on a reduced reference model, which is augmented by a neural element. This adaptive term is trained on-line to reduce the mismatch between plant and reduced model. As the wind turbine operates, the reduced model learns the characteristics of the system through its adaptive nature. This improves the performance of the predictive controller, and has the potential for automatically correct for modified environmental conditions or modified parameters of the machine, and might reduce the need for manually tuning and adjusting the controller for each different installation.

We have tested the performance of the adaptive model predictive controller, using a numerical approach for the solution of the regulation problem based on the direct transcription method. While this approach is computationally demanding, it provides a benchmark against which to compare the performance of a neural controller currently under advanced state of development by our group.

The results obtained during this investigation are encouraging. In particular, it appears that NMPC has the potential for reducing over-shoots and response time due to strong gusts. Furthermore, is also appears that the NMP controller allows for smoother operation in turbulent wind. Although the results of these aeroelastic simulations are promising, it is clear that only a real-time implementation and testing on actual turbines could demonstrate if substantial performance improvements of the NMPC approach over standard controllers are indeed possible.

REFERENCES

[1] *Wind turbine generator system — Part 1: Safety requirements*. International Standard IEC 61400-1, 1999.

[2] A. Barclay, P.E. Gill, J.B. Rosen. SQP methods and their application to numerical optimal control. Report NA 97–3, Department of Mathematics, University of California, San Diego, CA, 1997.

[3] O.A. Bauchau, C.L. Bottasso, L. Trainelli. Robust integration schemes for flexible multibody systems. *Computer Methods in Applied Mechanics and Engineering*, **192**, 395–420, 2003.

[4] O.A. Bauchau, C.L. Bottasso, Y.G. Nikishkov. Modeling rotorcraft dynamics with finite element multibody procedures. *Math. Comput. Modeling*, **33**, 1113–1137, 2001.

[5] J.T. Betts. *Practical methods for optimal control using non-linear programming*. SIAM, Philadelphia, 2001.

[6] C.L. Bottasso, C.-S. Chang, A. Croce, D. Leonello, L. Riviello. Adaptive planning and tracking of trajectories for the simulation of maneuvers with multibody models. *Computer Methods in Applied Mechanics and Engineering*, to appear in the special issue "Computational Multibody Dynamics", 2005.

[7] C.L. Bottasso, L. Riviello. Trimming of multibody rotorcraft models by a neural model-predictive auto-pilot. ECCOMAS Multibody Dynamics 2005, Madrid, Spain, June 21–24, 2005.

[8] L. Fausett. *Fundamentals of neural networks*. Prentice Hall, New York, NY, 1994.

[9] R. Findeisen, L. Imland, F. Allgöwer, B.A. Foss. State and output feedback nonlinear model predictive control: An overview. *European Journal of Control*, **9**, 190–206, 2003.

[10] K. Hornik, M. Stinchombe, H. White. Multi-layer feed-forward networks are universal approximators. *Neural Networks*, **2**, 359–366, 1989.

[11] D.A. Peters, C.J. He. Finite state induced flow models — Part II: Three-dimensional rotor disk. *Journal of Aircraft*, **32**, 323–333, 1995.

[12] D.M. Pitt, D.A. Peters. Theoretical prediction of dynamic inflow derivatives. *Vertica*, **5**, 21–34, 1981.

[13] S.R.J. Powles. The effects of tower shadow on the dynamics of a horizontal-axis wind turbine. *Wind Engineering*, **7**, 26–42 1983.

[14] S.J. Qin, T.A. Badgwell. An overview of industrial model predictive control technology. In J.C. Kantor, C.E. Garcia, B. Carnahan, Eds., Fifth International Conference on Chemical Process Control – CPC V, American Institute of Chemical Engineers, 232–256, 1996.

[15] S.J. Qin, T.A. Badgwell. An overview of nonlinear model predictive control applications. In F. Allgöwer, A. Zheng, Eds., Nonlinear Predictive Control, Birkhäuser, 369–393, 2000.

[16] D.E. Rumelhart, G.E. Hinton, R.J. Williams. Learning internal representations by error propagation. In D.E. Rumelhart, J. McClelland, Eds., Parallel Data Processing, **1**, 318–362, 1986.